IOPscience iopscience.iop.org

Home Search Collections Journals About Contact us My IOPscience

Electronic structure of beta -SiC surfaces

This article has been downloaded from IOPscience. Please scroll down to see the full text article.

1995 J. Phys.: Condens. Matter 7 1069

(http://iopscience.iop.org/0953-8984/7/6/010)

View the table of contents for this issue, or go to the journal homepage for more

Download details:
IP Address: 171.66.16.179
The article was downloaded on 13/05/2010 at 11:53

Please note that terms and conditions apply.

J. Phys.: Condens. Matter 7 (1995) 1069–1099. Printed in the UK

Electronic structure of β-SiC surfaces

Xiao Hu†, Hong Yan†, Masanori Kohyama‡ and Fumio S Ohuchi†

† Department of Materials Science and Engineering, FB-10, University of Washington, Seattle, WA 98195, USA

‡ Department of Materials Physics, Osaka National Research Institute, AIST, 1-8-31, Midorigaoka, Ikeda, Osaka 563, Japan

Received 29 April 1994, in final form 7 November 1994

Abstract. We have investigated the surface electronic structures of β-SiC reconstructed (001) surfaces for all the proposed models using a non-self-consistent tight-binding method. A new set of tight-binding parameters is introduced to calculate the β-SiC bulk and surface band structures. A Keating type empirical potential is used to obtain the relaxed (001) surface reconstructions for our band structure calculations. Distinct surface electronic characteristics corresponding to different surface structures are discussed based on the interpretation of surface density of states and electronic charge redistribution. Comparisons to the Si(001) surface are made with emphasis on the surface structure and bonding characteristics. We have also performed the electronic structure calculation for the ideal β-SiC(111) and (110) surfaces for the purpose of comparison. Our findings are in good agreement with most available experimental results and theoretical calculations.

1. Introduction

Special characteristics of silicon carbide (SiC), such as its wide band gap, high electron saturation velocity, and high thermal, mechanical, and chemical stability, have drawn increasing attention to studying its properties and applications in high-temperature, high-frequency, and high-power semiconductor devices [1–5]. On the other hand, SiC is one of the most important ceramic components in high-temperature structural materials systems, in which its joining to metals or other ceramics is frequently utilized to optimize the overall properties of the systems [6–9]. Therefore, the structure and properties of SiC surfaces and its interfaces with other materials become a very important issue.

SiC has a variety of structures with different stacking sequences of close-packed Si and C layers, all but one of which are classified as α-SiC with hexagonal or rhombohedral symmetries. β-SiC, however, has a cubic (zincblende) crystal structure and is of more interest in its properties and applications in semiconductor device technologies. In this paper, we focus our attention on the electronic properties of β-SiC surfaces.

The β-SiC(001) surface has been observed to have rich surface reconstruction patterns in experiments [1, 10–17]. Several theoretical studies of energetics and atomic configurations of the β-SiC surface structure have been reported in the literature [18–25]. A variety of reconstruction models have been proposed by both experimentalists and theorists [1, 11–14, 16, 19, 20, 24, 56]. Much attention has been paid to (2×1), (3×2), and $c(2 \times 2)$ reconstructed surfaces. In this paper, a widely accepted Si dimer array model for the (2×1) surface is used. A model for the (3×2) surface proposed by Hara *et al* [11, 12] is adopted. For the $c(2 \times 2)$ surface, we have examined two different models, namely the staggered model and the bridged model proposed by Bermudez and Kaplan [16] and Powers

0953-8984/95/061069+31$19.50 © 1995 IOP Publishing Ltd

et al [20], respectively. Detailed experimental observations and proposed models for these reconstructions will be described in section 3.

Notably, the (2×1) reconstruction of the β-SiC(001) surface is analogous to the Si(001) (2×1) surface, on which an Si dimer array model is also favoured by extensive experimental and theoretical investigations [26–29]. The $c(2\times 2)$ reconstruction, which is observed on the β-SiC(001) C terminated surface, however, has not been reported for Si(001), indicating the different surface characteristics between the Si(001) and the β-SiC(001) C terminated surfaces. The complexities on the β-SiC(001) surface, such as the existence of ionicity and multiple elements, make the comparison of the surface atomic and electronic structures between the Si(001) and β-Si(001) surfaces very interesting. In this paper, the Si(001) surface will serve as a counterpart of the β-SiC(001) surface for the purpose of comparison.

Different surface structures will have different electronic characters. Many of the experimental studies of the atomic structures of the β-SiC surfaces, using a variety of surface analysis techniques, have also investigated their core level electronic structures, which provide indications of structure related changes in bonding. Detailed examinations of the valency electronic structures of the β-SiC($00\bar{1}$) surfaces have been carried out by Parrill and Bermudez [30] and Hoechst *et al* [31] using photoemission techniques. From valency band photoemission spectra, Parrill and Bermudez have found evidence for the existence of surface resonance, and that surface states might exist at the upper edge of the valency band. More detailed angular resolved valency band photoemission spectra obtained by Hoechst *et al* [31] have shown that a surface state was located at about 1.0 eV above the valency band maximum. For β-SiC(111) and (110) surfaces, however, to our knowledge, no direct measurements of valency electronic structure have been made so far.

A few theoretical studies have been done for the valency electronic structures of the β-SiC surface [20–23]. Lu *et al* [23] have carried out an extended Huckel band calculation for the β-SiC(001) (2×1) surface. In their calculation, the relaxed dimer length is too large and the width of the valency band is much underestimated compared to most experimental data. On the other hand, Lee and Joannopoulos [22] have studied the electronic structure of both real and relaxed β-SiC(110) surfaces by using a transfer matrix method [32]. They find that for β-SiC(110) surfaces, if atomic relaxation is the only mechanism responsible for SiC surface atom rearrangement, the surface states should be in the fundamental gap, and that the surface states have dangling bond characters and are not as dramatically influenced by the relaxation as the back bond states.

This paper attempts, for the first time, to examine the surface structure related changes in bonding and electronic characteristics for all the relevant models of the β-SiC(001) reconstructed surfaces. A comparison to the Si(001) surface concerning surface configurations and bonding features has been made. In addition, in order to compare the different bonding and electronic characteristics associated with the corresponding β-SiC surface orientations, calculations of the ideal β-SiC(111) and (110) surface are also carried out. This work represents the first step of our systematic study of β-SiC surfaces and its interfaces with metals.

The method we use in this work is an empirical tight-binding (TB) technique [36, 39] with a new set of parameters. An empirical potential is employed to relax the reconstructed surface structures. Although a complete study of β-SiC surfaces requires a self-consistent total energy calculation, we believe, as we shall demonstrate later in this paper, that the method we use here represents a valid and efficient approach to explore the qualitative features of the β-SiC surface bonding and electronic structures.

The rest of this paper is organized as follows. Section 2 briefly describes the calculation methodology and the parameters we have used in this work. The following section discusses

the experimental observations and theoretical models of β-SiC(001) surface reconstructions. The results of our calculations are presented in section 4 with detailed discussions about the notable features. Finally, we summarize in section 5.

2. The method of calculation

2.1. The tight-binding method and its parameters

In our calculations, we have used the two-centre integral tight-binding model initially introduced by Slater and Koster [39]. The Hamiltonian matrix is now simplified by using the two-centre approximation. To represent the Hamiltonian matrix elements, we utilize the interatomic distance dependent functional forms proposed by Harrison and Froyen [36, 40]. The density of states (DOS) and the local density of states (LDOS), as well as the atomic charges, are then obtained in terms of the corresponding eigenenergies and eigenvectors. With this method, one can deal with complex structures containing many atoms in a large unit cell such as surface systems.

In general, this TB method, taking only the nearest-neighbour interactions into account and utilizing only the valency atomic orbitals as a minimum basis set, can reproduce the valency band reasonably well for a variety of semiconductors, although its representation of the conduction band and the fundamental gap is not satisfactory [33, 36, 37]. The main problem with the TB parameters is the limited size of the basis set; in particular, the absence of d states from the basis set leads to unfavourable energy states in zincblende structure materials and usually results in an incorrect indirect X conduction band minimum [33, 36, 37]. The inclusion of d states, or even a single excited s* state, which mimics the effects of the higher-lying d states, significantly improves this situation and leads to a more accurate description of the conduction bands and the energy gap [33, 41–43]. Recently, Robertson [38] has proposed a new set of universal parameters for SiC and hydrogenated amorphous SiC by incorporating the s* state, which gives a reasonably good overall band structure. In this work, we have also included an s* state in our basis set. Our parameters are derived from Vogl *et al*'s sp^3s^* Hamiltonian matrix elements [33] for β-SiC (see table 1), which are fitted to Hermstreet and Fong's calculated results [34]. Note that the interactions between anion s orbital and cation p orbital η_{sapc} and between cation s orbital and anion p orbital η_{scpa} are now non-degenerate. Our parameters are listed in table 1. Harrison's and Robertson's parameters can be found in [36] and [38], respectively.

Table 1. Universal two-centre integral TB parameters used in our calculations.

	E_s	E_p	E_s^*	$V(ss)$	$V(sapc)$	$V(scpa)$	$V(pp\sigma)$	$V(pp\pi)$	$V(s^*apc)$	$V(s^*cpa)$
C	−8.4537	2.1234	9.6534	−1.450	1.919	1.860	1.738	−0.337	1.763	0.891
Si	−4.8463	4.3466	9.3166							

Because of different experimental fitting data bases, our parameters are expected to be different from Robertson's. While his parameters underestimate the valency band width, our parameters may slightly overestimate the valency band width. Our result, however, is closer to that obtained by Talwar and Feng [35], who have used a large set of experimental data of the β-SiC valency band structures, including soft-x-ray emission, luminescence, optical reflectivity and the absorption technique for their fitting basis. Moreover, because

Table 2. Calculated eigenvalues of critical points in G, X, and L directions for bulk β-SiC.

Critical points	Our calculation	
Γ	−19.20	(Γ1v)
	0.00	(Γ15v)
	5.90	(Γ1c)
	6.47	(Γ15c)
X	−14.28	(X1v)
	−11.51	(X3v)
	−2.79	(X5v)
	2.35	(X1c)
	5.41	(X3c)
	9.26	(X5c)
L	−16.10	(L1v)
	−9.69	(L3v)
	−1.38	(L3v)
	3.56	(L1c)
	5.87	(L3c)
	7.85	(L1c)

the *diagonal* Hamiltonian matrix elements should be rescaled, or shifted, from the free atom orbital energies in a general fitting procedure, and the fitting of the *off-diagonal* matrix elements depends solely on the *diagonal* matrix elements and the lattice constants of the concerned materials, different rescaling, or shifting, of the free atom orbital energies will produce different fitting parameters. Robertson's [38] parameters were specified for the interactions between Si, C, and H elements, since his determination of the diagonal matrix elements was guided by the free atom orbitals of Si, C and H with necessary shifts and by the need for compatibility of the orbital energies associated with Si–Si, Si–C, Si–H, and C–H bonds. On the other hand, Vogl *et al* [33] rescaled their diagonal Hamiltonian elements uniformly for all the sixteen tetrahedrally bonded semiconductors they have investigated by setting the differences between the diagonal matrix elements proportional to the differences between the corresponding free atom orbital energies.

We point out that although the fitting procedures by Robertson and Vogl *et al* have the same essence, the parameters that we have derived from Vogl *et al*'s Hamiltonian matrixes can be employed to study the interactions between different semiconductors or different elements within these semiconductors. In the cases when the parameters for the interaction between two elements are not specifically fitted within a semiconductor, the Vogl *et al* universal parameters [33, 37] can then be used. This may be the major advantage of our parameters over Robertson's for further studies of β-SiC surfaces and its interfaces with other materials.

Table 3. A comparison of important optical gaps (in electronvolts) in β-SiC.

Transition	Experiment[a]	Present work	[34]	[35]	[52]	[57]	[58]	[58]
Γ_{15v}–Γ_{1c}	6.00	5.90	5.92	6.00	6.50	5.90	5.14	6.80
Γ_{15v}–X_{1c}	2.417	2.35	2.35	2.40	2.40	2.30	2.40	2.70
Γ_{15v}–Γ_{15c}		6.47	6.49	7.00	7.20	7.80	10.83	8.60
X_{1c}–X_{3c}	3.05	3.06	3.08	3.29	3.70	2.60	3.24	3.20
L_{3v}–X_{1c}	4.20	3.73	3.90	4.40	3.10	3.10	3.26	6.00

[a] Experimental data taken from [35] table III.

Our calculated eigenvalues at critical points for bulk β-SiC are given in table 2. The comparison of experimental measurements of optical gaps with our calculated results and those of others is given in table 3. We see that our simple TB parameters reproduce the features of the electronic structure of bulk β-SiC quite well.

Our calculated band structure for β-SiC bulk and the corresponding total DOS and LDOS are shown in figure 1. The lowest valency band of β-SiC, i.e. band 1 (figure 1(A)) consists mainly of C 2s and Si 3s and 3p characters (figure 1(C) 'c', figure 1(D) 'f'). This band is largely due to the interaction between the C 2s orbital and the Si 3s orbital. The Si 3s orbital is more hybridized with the Si 3p orbital than the C 2p orbital with the C 2s; this is because, in principle, the larger the difference in energies between the atomic s and p orbitals, the less energetically favourable it is to build s–p hybrids. Since C has a larger difference between atomic 2s and 2p orbital ($E_p - E_s = 10.68$ eV) than Si does between 3s and 3p orbitals ($E_p - E_s = 9.19$ eV), it is expected that C is less s–p hybridized than Si. Band 3 and band 4 (figure 1(A)) have mixed C 2s, 2p and Si 3s, 3p characters. These states (figure 1(C) 'b'; figure 1(D) 'e') are due to the interactions among C 2s and 2p states and Si 3s and 3p states. The uppermost valency band (figure 1(A)), corresponding to peaks of figure 1(C) 'a' and figure 1(D) 'd', is produced by the interaction between almost pure C 2p and Si 3p orbitals. The band gap, indirect to the X_1 conduction state, is 2.35 eV. Finally, the conduction band is basically formed from the antibonding states of the corresponding bonding states in the valence band. It should be pointed out that, although our calculated value of the effective atomic charge of the bulk β-SiC, 0.6, is larger than the experimental value of 0.41, it compares better than Robertson's result of 0.18. We notice that the effective atomic charge, or the orbital occupancy, is extremely sensitive to the shape of the band structure.

2.2. The calculation method for the surface

The surface electronic structures are calculated by using slab unit cells. The slab configurations, as well as the associated two-dimensional Brillouin zone, for the ideal β-SiC(001), (111), and (110) surfaces are shown in figures 2, 3 and 4, respectively. The periodicity in the x, y directions is maintained, while the periodicity in the z direction is considered to be infinite. By sampling $k(k_x, k_y)$ in the two-dimensional Brillouin zone (2DBZ) projected from the three-dimensional Brillouin zone (3DBZ) in the z direction (normal to the surface of interest), the projected bulk and surface eigenvalues and eigenvectors at each $k(k_x, k_y)$ are obtained. The LDOS is computed by using four or nine wave vectors in the irreducible part of the 2DBZ with Gaussian broadening of a 0.2 eV full width at half maximum. It should be pointed out that for all the reconstructed (001) surfaces, the same 2DBZ is used for sampling k vectors for computational convenience, although the real irreducible parts of the 2DBZs of different reconstructed surfaces are different and usually smaller than that of the ideal surface.

For the (001) surface (figure 2), the slab unit cell contains five layers of Si (or C), in total 20 Si (or C) atoms, and six layers of C (or Si), in total 24 C (or Si) atoms with C (or Si) atoms present on two equivalent surfaces if the investigated surface is terminated with C (or Si). As mentioned before, to preserve simplicity and to allow easy identification of chemical trends in the band structure for different surfaces, we take only the nearest-neighbour atomic interaction into consideration. All the bond lengths are obtained by performing an energy minimization for a specific slab unit cell, which will be discussed in the following section. Since the Hamiltonian matrix elements are two-centre integral parameters (table 1) and r^{-2} interatomic distance dependent, the Hamiltonian matrix can now be established. We notice that the parameters for the interaction between anion carbon s (or s*) orbital and cation silicon p orbital, η_{sapc} (or $\eta_{\mathrm{s^*apc}}$), and between cation silicon s (or s*) orbital and anion

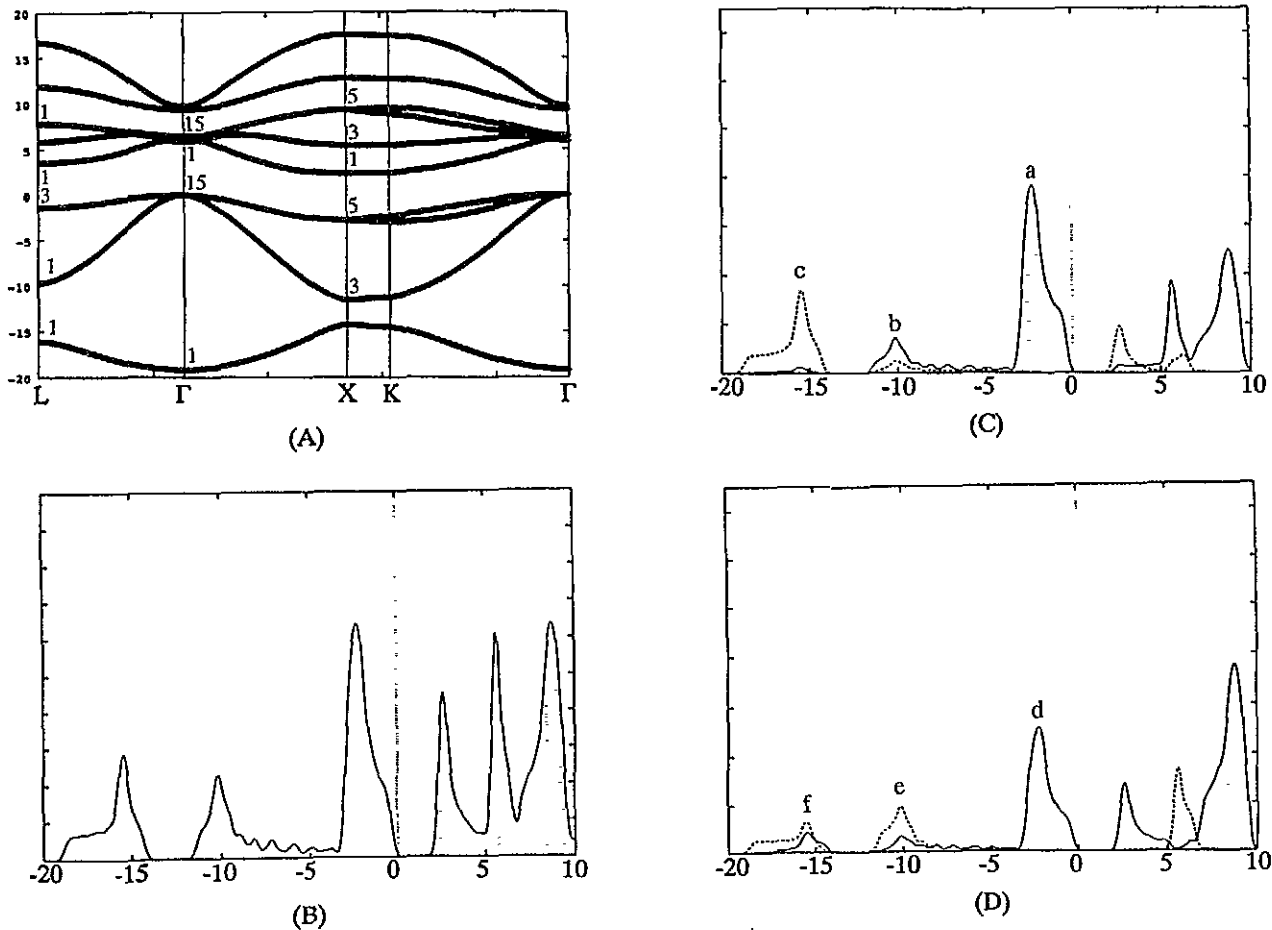

Figure 1. β-SiC bulk electronic structure: solid lines are p-like orbitals and dashed lines are s-like orbitals. (*A*) Bulk β-SiC band structure; (*B*) total DOS of bulk β-SiC; (*C*) LDOS of C; (*D*) LDOS of Si.

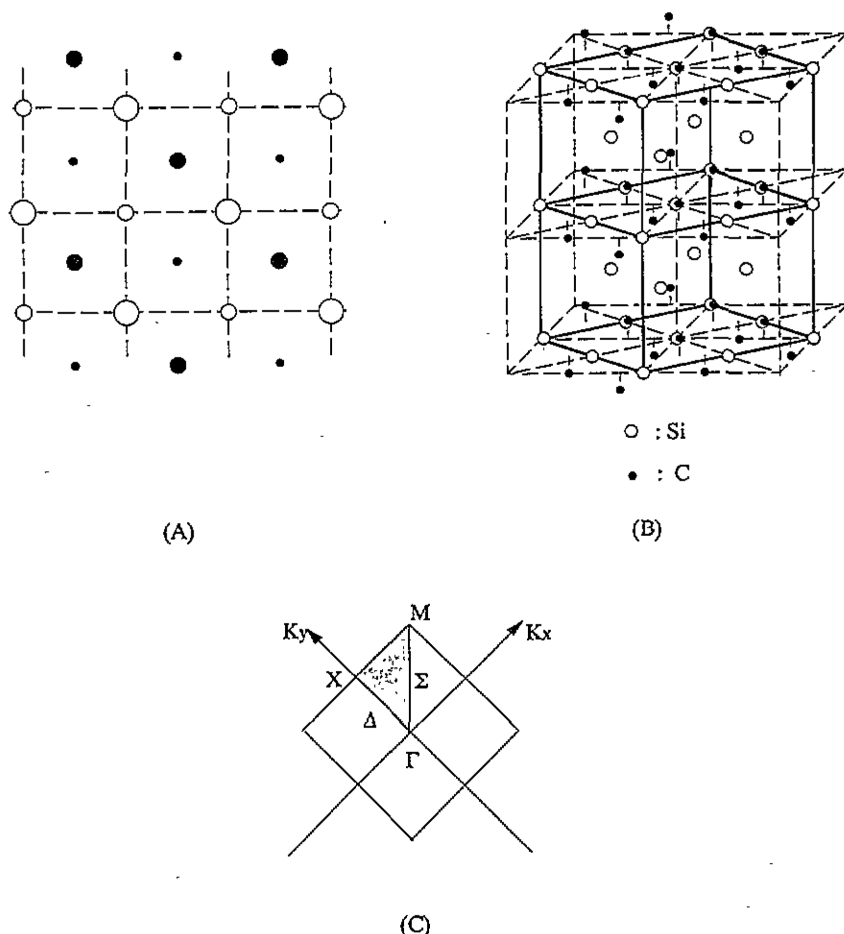

Figure 2. The β-SiC(001) ideal surface structure: (*A*) the top view of the ideal (001) surface; (*B*) the slab unit cell used in our calculation; (*C*) the two-dimensional Brillouin zone projected from the (001) direction (the shaded area is an irreducible part of the 2DBZ).

carbon p orbital, η_{scpa} (or η_{s^*cpa}) are distinguished. For Si–Si and C–C bonds, however, there exists no such difference and the parameters between s (or s*) orbital and p orbital are determined by taking the average of η_{sapc} and η_{scpa} (or η_{s^*apc} and η_{s^*cpa}).

The slab cell of the ideal (111) surface (figure 3) contains six C atoms and six Si atoms. The (111) surface, like the (001) surface, is a polar surface, but its slab unit cell is different from that of the (001) surface. In the (001) slab unit cell, both surfaces have the same element, either Si or C; while in the (111) surface case, the two slab surfaces cannot be equivalent, one is C terminated and the other Si terminated. The LDOSs for the two surface layers are computed separately and because there are 10 layers of atoms in between the surfaces, the interference between these two surfaces is negligible.

From the (110) surface (figure 4), the slab unit cell, which has an equal number of atoms in the same layer, contains five layers of Si and C. Each layer contains two Si atoms and two C atoms, in total there are 10 Si atoms and 10 C atoms in the unit cell. The 2DBZ for the ideal (110) surface of the zincblende structure is also illustrated in figure 4.

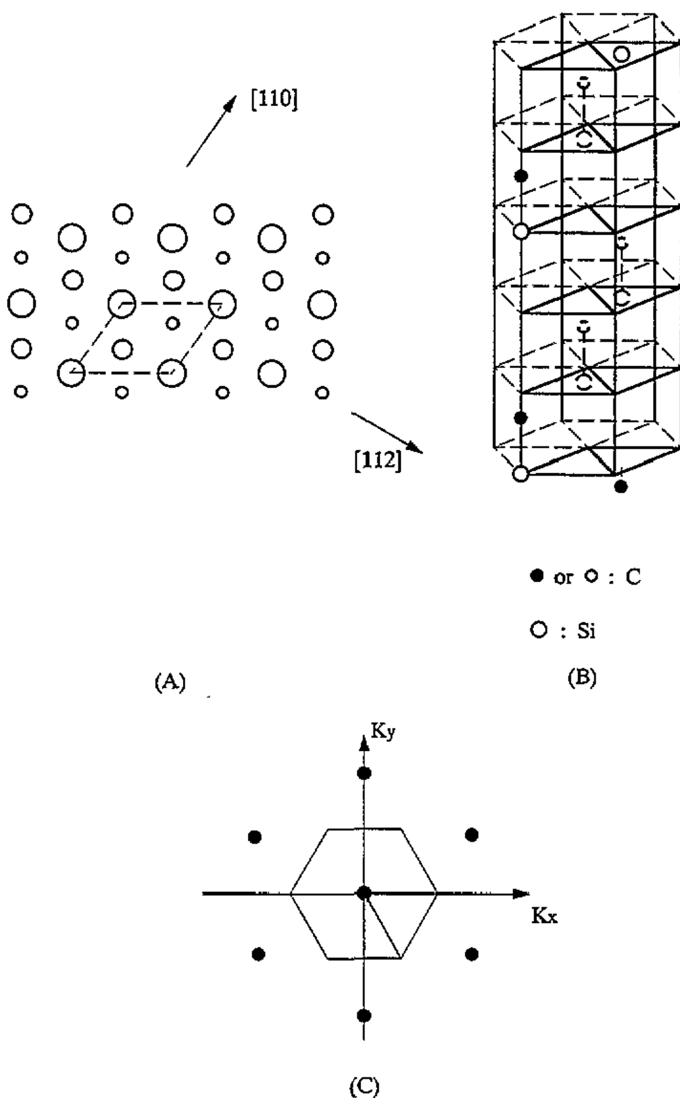

Figure 3. The β-SiC(111) ideal surface structure: (*A*) the top view of ideal (111) surface (circles are doubly projected Si and C); (*B*) the slab unit cell used in our calculation; (*C*) the two-dimensional Brillouin zone projected from the (111) direction (the shaded area is an irreducible part of the 2DBZ).

3. Surface reconstructions

3.1. Experimental observations

β-SiC(001) surface reconstruction patterns include (3×2) [10–17, 20] (occasionally observed as (3 × 1) [10]), (5 × 2), (2 × 1), c(4 × 2), c(2 × 2), and (1 × 1) in order of decreasing surface Si concentration. Typically, a clean, well ordered β-SiC(001) surface is obtained by annealing an epitaxially grown β-SiC sample exposed to Si flux at 850–1100 °C. Although the specific temperature and exposure time determine the resulting SiC surface composition,

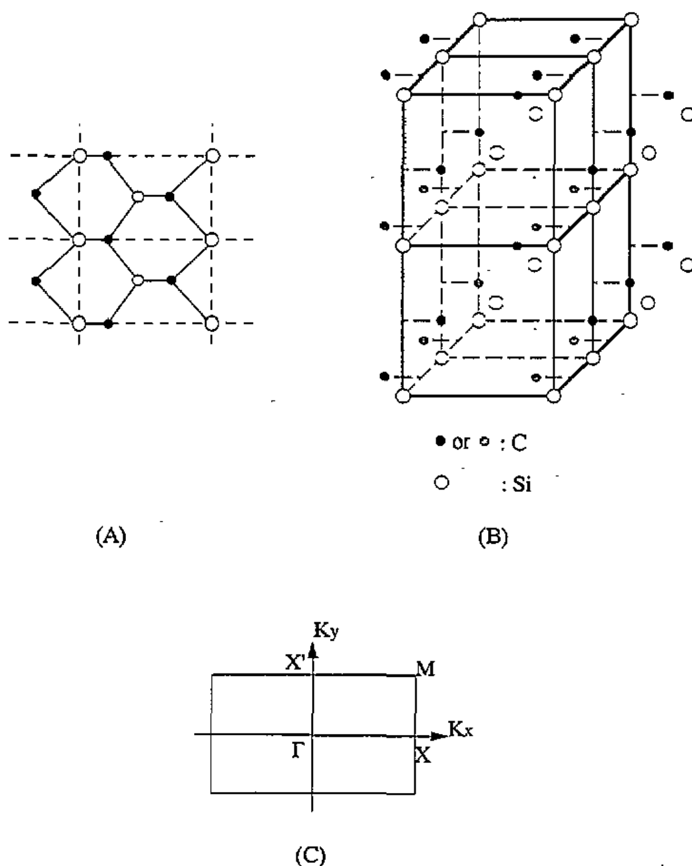

Figure 4. The β-SiC(110) ideal surface structure: (*A*) the top view of the ideal (110) surface; (*B*) the slab unit cell used in our calculation; (*C*) the two-dimensional Brillouin zone projected from the (110) direction (the shaded area is an irreducible part of the 2DBZ).

an Si rich surface is usually produced. This surface is associated with (2×1) or $c(4 \times 2)$ reconstructions, and is believed to be terminated with one monolayer (ML) of Si atoms. While Kaplan [14] has found that $c(4 \times 2)$ can be observed at temperatures as high as 600 °C, studies of both Parrill and Chung [10] and Hara *et al* [11, 12] have also reported that leaving the $c(4 \times 2)$ surface at room temperature will result in a (2×1) pattern, but all authors agree that these two surface phases have the same composition and a basic Si–Si dimer structure, with the $c(4 \times 2)$ being a modification to the (2×1) surface.

Adsorption of excess Si on the (2×1) (or $c(4\times2)$) surface at relatively lower temperature (< 750 °C) will lead to (3×2) or (5×2) reconstruction [11–17, 20]. This surface has the highest Si/C surface composition ratio. The strongest indication of Si–Si bonding is found on this surface.

A C terminated $c(2 \times 2)$ surface can be prepared either by annealing the (2×1) surface at relatively higher temperature (> 1200 °C) in ultrahigh vacuum, or by adsorption of excess C on the same initial surface [11–17, 20]. Experiments have found a feature characteristic of surface graphite and evidence of disappearance of Si–Si bonding and formation of C–C bonding.

3.2. Proposed reconstruction models

The β-SiC(001) (2×1) or $c(4 \times 2)$ surface is considered to be analogous to Si(001) and Ge(001) surfaces, which also present (2×1) and $c(4\times 2)$ reconstructions, as well as $p(2\times 2)$ etc. Different experiments observe different reconstructions of Si(001). It is likely that some of the surfaces are metastable and stabilized by the presence of impurities. Different theoretical calculations have also predicted different reconstructions of the lowest energy, but the energy differences are usually very small. Since the β-SiC(001) (2×1) surface, in analogy to the Si(001) surface, is believed to consist of Si dimer units, and $c(4 \times 2)$ is a different arrangement of the Si dimers with respect to the (2×1) surface, this work, as in other studies, has focused on the model for (2×1) in order to reveal the bonding characteristics of these surface reconstructions. Powers *et al* [20] have analysed the β-SiC(001) (2×1) surface by performing a dynamic calculation with the automated tensor LEED (low-energy electron diffraction) method. Their result indicates that the surface is terminated by 1 ML of Si atoms, forming asymmetric buckled dimers. This result is in agreement with all the experimental work, as well as with the calculations performed by Craig and Smith [24], using a semi-empirical slab MINDO method, and by Mehandru and Anderson [21], who have performed semi-empirical TB ASED band calculations using finite-sized cluster models. The atomic configuration of this model is displayed in figure 5.

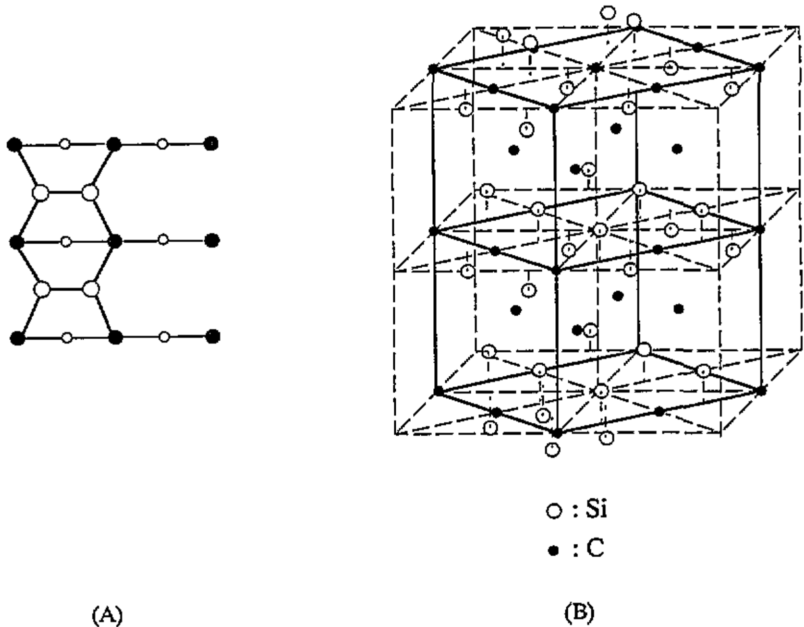

Figure 5. The Si terminated (001) (2×1) surface structure: (*A*) the top view of the reconstruction; (*B*) the slab unit cell used in our calculation.

The model for the β-SiC(001) (3×2) surface was originally proposed by Dayan [1], inspired by Pandey's [45] defect model for the Si(001) (2×1) surface. Kaplan [14] adopted this model to interpret his LEED patterns of the β-SiC(001) surface. In Dayan's model of the (3×2) surface, dimer vacancies are arranged periodically in rows, and the ideally Si terminated surface is topped by an additional $\frac{2}{3}$ ML of Si. The addition of the atomic Si

layer on the surface leads to a rotation of the dimer orientation by 90°, which is evident in Kaplan's LEED patterns of (3×2) and (2×1) surfaces. However, more careful experiments have demonstrated that the (3×2) surface is associated with $\frac{1}{3}$ ML excess Si rather than $\frac{2}{3}$ ML [11, 12, 17]. As a modification to Dayan's model, Hara *et al* [11, 12] suggested a model for the (3×2) phase in which every third row of Si dimers is present between two vacancy rows on the (2×1) surface. We choose Hara *et al*'s model for the electronic structure calculation of the (3×2) surface. The surface structure and the slab unit cell of this model are illustrated in figure 6.

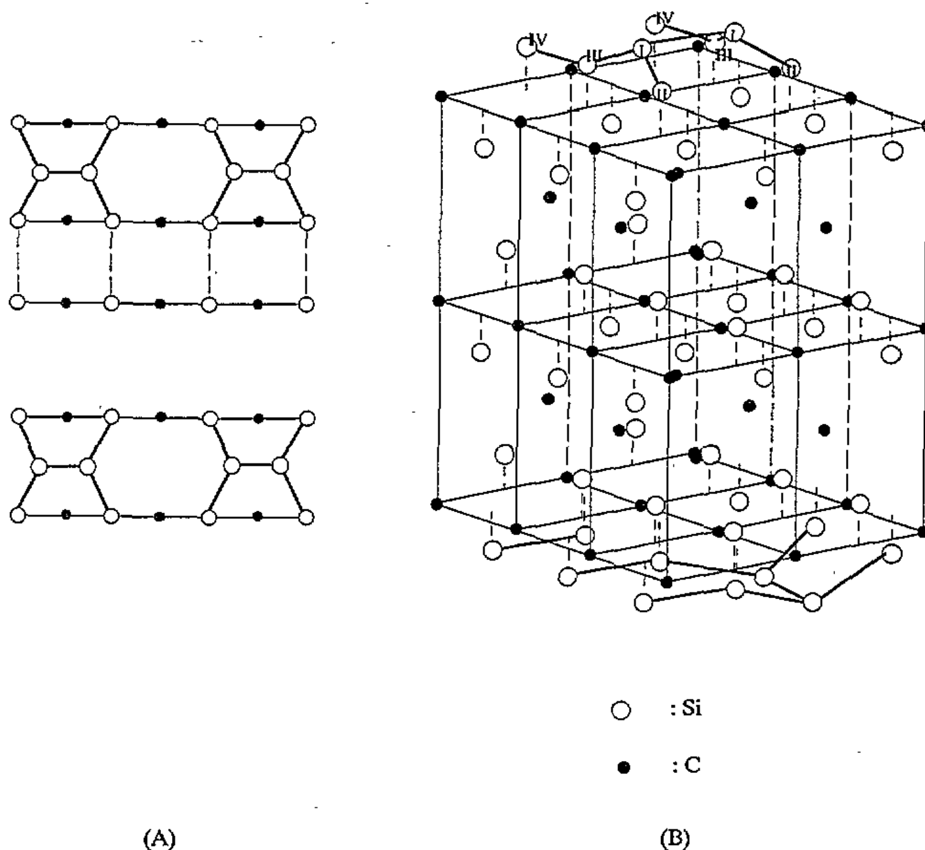

Figure 6. The Si terminated (001) (3×2) surface structure: (*A*) the top view of the reconstruction; (*B*) the slab unit cell used in our calculation.

There are two different models proposed for the β-SiC(001) $c(2 \times 2)$ surface. One is suggested by Bermudez and Kaplan [16], based on Auger and electron energy loss spectroscopies, LEED, and electron stimulated desorption of H^+ from the surface. They proposed a staggered '>C–C<' unit model, shown in figure 7. In this model, each C atom bridges two surface Si atoms and each C has a single dangling bond on the surface. The calculation of Craig and Smith [56], employing a slab MINDO method, also favours this model, but it gives a C double dimer bond on a clean surface.

The other model was proposed by Powers *et al* [20]. They prepared their samples in two different ways; removal of the surface Si by high-temperature annealing in ultrahigh

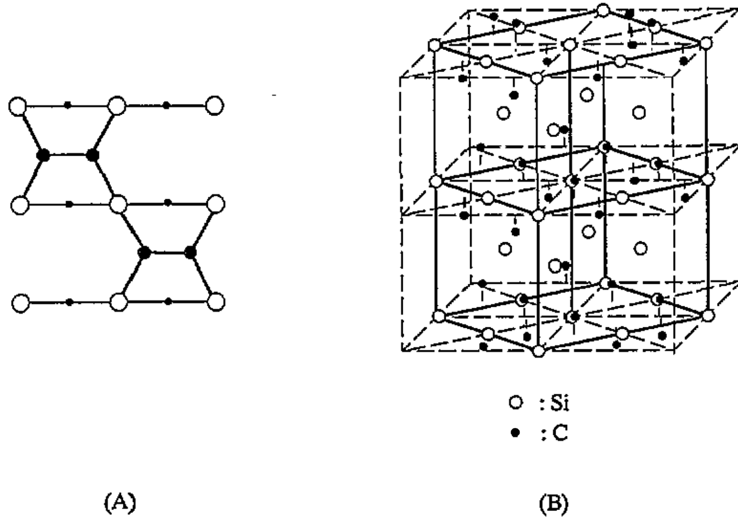

Figure 7. The C terminated (001) (2 × 2) surface structure—the staggered model: (*A*) the top view of the reconstruction; (*B*) the slab unit cell used in our calculation.

vacuum, and deposition of surface C by exposing the (2 × 1) surface to C_2H_4 at 1125 °C. As they had done for the (2 × 1) surface, they obtained the optimized surface configuration using their automated search method based on tensor LEED. For both samples, their analysis gives a surface terminated with a single monolayer of C atoms forming '–C=C–' bridges between two of the second-layer Si atoms. Weak Si dimer bonds are found in the second layer of the c(2 × 2) surface produced by Si sublimation, but not for the c(2 × 2) surface produced by C_2H_4 exposure. Their conclusion qualitatively agrees with Badziag's prediction based on a self-consistent total energy MNDO (modified neglect of diatomic overlap) calculation of a cluster model [19], except for the details of the sub-layer atomic geometry. This model is illustrated in figure 8.

3.3. The determination of the surface structure for the band structure calculations

In order to obtain the relaxed surface geometry of β-SiC for use in our DOS calculations, we have carried out energy minimization for the various slab units corresponding to the above-described reconstruction models, using a valence force field (VFF) model of the Keating type [49, 50]. In this method, the change in total elastic deformation energy $E_{\rm tot}$ can be expressed as [46, 47]

$$E_{\rm tot} = \sum_i E_i$$

where E_i is the elastic energy of atom i and is expressed as

$$E_i = \sum_{j \neq i} \frac{3\alpha_{ij}}{16 r_{ij}^{0\,2}} (r_{ij}^2 - r_{ij}^{0\,2})^2 + \sum_{(j,k) \neq i} \frac{3\beta}{8 r_{ij}^0 r_{ik}^0} (\boldsymbol{r}_{ij} \cdot \boldsymbol{r}_{ik} + \tfrac{1}{3} r_{ij}^0 r_{ik}^0)^2$$

where j and k are the nearest-neighbour atoms of i; the first sum is performed over all the nearest neighbours of atom i, and the second sum over all the nearest-neighbour pairs (j, k) of atom i; r_{ij}^0 and r_{ik}^0 are the equilibrium interatomic distances; $\boldsymbol{r}_{ij}$ and $\boldsymbol{r}_{ik}$ are the vectors

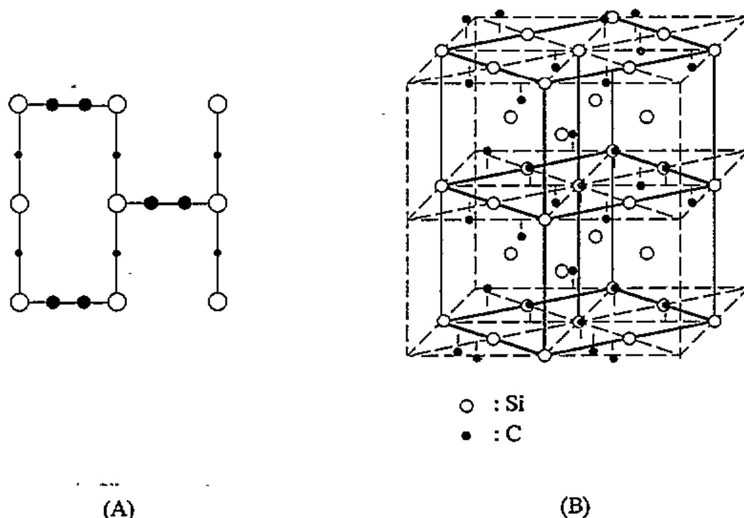

Figure 8. The C terminated (001) (2×2) surface structure—the bridged model: (*A*) the top view of the reconstruction; (*B*) the slab unit cell used in our calculation.

connecting atom i and its nearest neighbours j and k and α_{ij} and β are bond stretching and bond bending force constants, respectively. In this work, we use the force constants obtained by Martins and Zunger [46]. α_{ij} for Si–C, C–C, and Si–Si bonds are the parameters for the bulk SiC, diamond, and Si crystal, respectively, while β is all the same as that for SiC. The parameters have been shown to be able to generate similar configurations of the β-SiC{122}$\Sigma = 9$ grain boundaries to those obtained by the self-consistent TB method [47, 51]. All the atoms in a slab are subjected to relaxation. After the convergence of the total elastic energy only the topmost layer and the sublayer atoms turn out to have significant displacements with respect to their ideal bulk atomic positions. Our calculated dimer lengths and vertical height variations for β-SiC(001) surfaces are listed in table 4, in comparison with the results of Powers *et al* [20], Mehandru and Anderson [21], Craig and Smith [24],and Badziag [19]. Besides the work cited in table 4, Lu *et al* [23], using a Keating model with different parameters and functional forms, have obtained an Si dimer length of 2.664 Å and a C dimer length of 1.974 Å for the β-SiC(001) (2×1) surface, which are somewhat too large.

We are interest in the ideal (111) and (110) surfaces only as a contrast to the (001) surfaces of complex reconstructions in order to clarify the distinctive characteristics of the electronic structures of these reconstructed (001) surfaces. Therefore these ideal surfaces are not subjected to relaxation. Illustrations of the surface structures of the ideal (111) and (110) surfaces are shown in figures 3 and 4, respectively.

4. The surface density of states and surface charge redistribution

4.1. The β-SiC(001) ideal C terminated surface

For the C terminated β-SiC(001) ideal surface (figure 2), the total DOS and the LDOS are shown in figure 9. Since the total DOS is defined as the sum of the LDOSs of the specified atomic layers, or groups, within the slab unit cell, the shape of the total DOS depends on

Table 4. A comparison of our calculated dimer length and vertical height variations with Powers *et al* [20] and Mehandru and Anderson's results [21]. Δh is the vertical height changes ($\Delta h = h - h_0$) with reference to ideal bulk atomic positions (in ångströms).

	Models against calculations	Si terminated		C terminated	
		(2 × 1) Si dimer	(3 × 2) Si dimer	(2 × 2) staggered C dimer	(2 × 2) bridged C dimer
Dimer length	This work	2.38	2.36	1.65	1.54[a]
	Powers *et al* [b]	2.31	—	1.32	1.25
	Mehandru and Anderson[c]	2.16	—	—	—
	Craig and Smith [d]	2.33/2.47[e]	—	1.37/1.584[e]	—
	Badziag[f]	2.40	—	—	1.21/1.33[e]
Δh	This work	−0.043	0.345	−0.173	0.529
	Powers *et al* [b]	−0.1/0.12[g]	—	0.14	0.53
	Mehandru and Anderson[c]	−0.04	—	—	—
	Craig and Smith[d]	−0.13/−0.33[g]	—	0.41/0.23[e]	—
	Badziag[f]	—	—	—	—

[a] Diamond C–C bond length.
[b] Dynamic calculation with an automated tensor LEED method.
[c] Semi-empirical TB atomic superposition and electron delocalization (ASED) band calculation using finite-sized cluster models.
[d] Semi-empirical slab–MINDO molecular orbital method.
[e] The first value is obtained on a clean surface; the second value is obtained on a monohydride surface.
[f] Self-consistent total energy MNDO cluster calculation.
[g] Buckled dimer atoms.

the size of the slab. A larger number of bulk atoms will give a more bulk like total DOS. In principle, the appearance of electronic density of states in the energy band gaps is due to the change of atomic environment at surface. In the present case, each C atom in the first layer interacts with only two Si atoms, and the resultant energy bands of those surface layers, including both the first C layer and the second Si layer, do not completely expand into the bulk energy bands.

The important feature of this surface is that the first-layer C has a C 2p dangling bond state located at about 2.0 eV. The dangling bond state (figure 9(B) 'a') is an almost pure C 2p orbital state (table 1), rather than a hybridized sp^3 state. This is because each surface C has two covalent bonds with Si in the sublayer and two dangling bonds, therefore the environment for tetrahedral sp^3 hybridization is not satisfied. In contrast, on the ideal (111) surface (figure 3), where each surface atom loses one of its four tetrahedral nearest neighbours, it is expected that the electronic states of the (111) surface atoms can be best understood by using sp^3 hybrid orbitals, and the dangling bond state should be close to a dangling sp^3 state. This has been verified by the calculated DOS for the (111) C terminated surface, where the dangling state (figure 11(B) 'a') is a mixture of C 2s and 2p orbitals and located at a much lower energy level with respect to the pure C 2p orbital level. Details of the electronic structure of the (111) C surface will be discussed in subsection 4.3. In addition, on the (001) C surface, the broadening of the peak 'a' in figure 9(B) can be attributed to the coupling of the dangling bonds both of the same atom and of different surface atoms.

The hybridized surface resonance state (figure 9(B) 'b'; (figure 9(C) 'd') is centred at about 0.0 eV, extending the valence band up to 1.0 eV in the fundamental gap. It is a mixture of C 2p ($\sim$ 60%), C 2s ($\sim$ 15%), and Si 3p ($\sim$ 25%) orbitals, indicating that this state is due to the interaction between dangling bonds and back bonds (bonds between

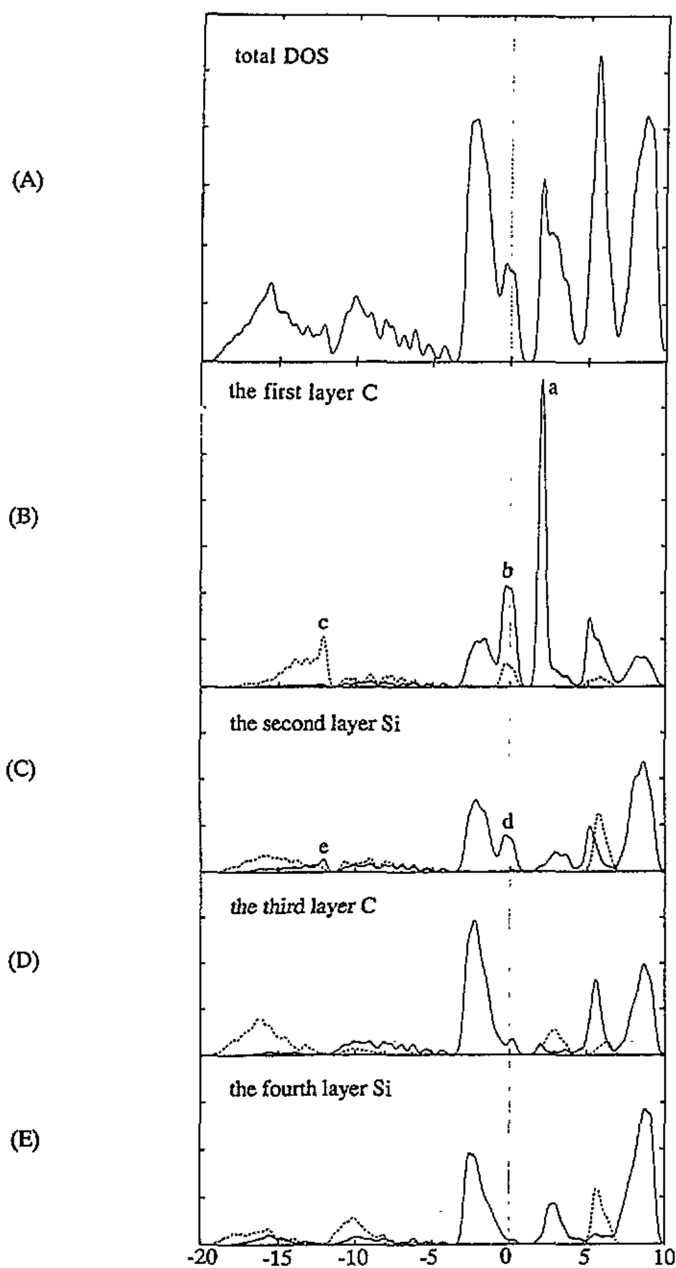

Figure 9. The DOS of the β-SiC(001) ideal C terminated surface; solid lines are p-like orbitals and dashed lines are s-like orbitals. (*A*) The total DOS; (*B*) the LDOS of the first-layer C; (*C*) the LDOS of the second-layer Si; (*D*) the LDOS of the third-layer C; (*E*) the LDOS of the fourth-layer Si.

surface C and second-layer Si). The Fermi energy (defined as the highest occupied energy level in this paper) is at about 0.5 eV, therefore the resonance state is partially filled and the dangling state is completely empty, giving the surface a metallic character.

The ionicity gap is almost completely filled, with first-layer C 2s character ($\sim$ 85%),

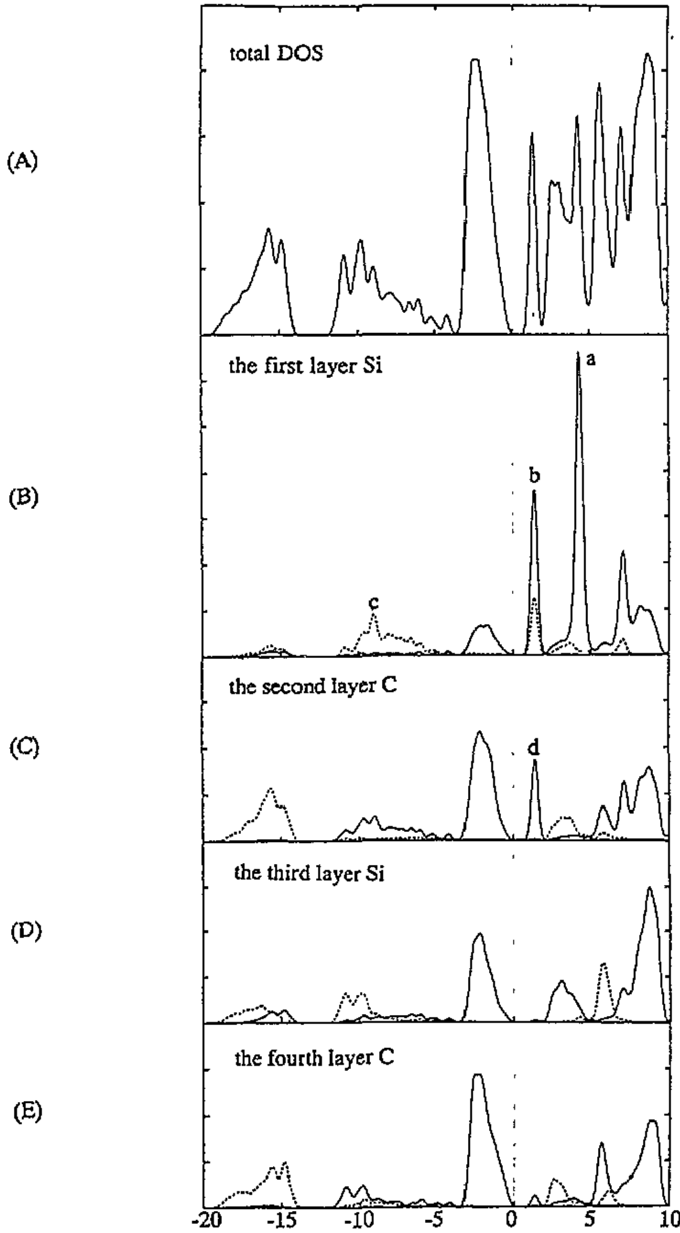

Figure 10. The DOS of the β-SiC(001) ideal Si terminated surface; solid lines are p-like orbitals and dashed lines are s-like orbitals. (*A*) The total DOS; (*B*) the LDOS of the first-layer Si; (*C*) the LDOS of the second-layer C; (*D*) the LDOS of the third-layer Si; (*E*) the LDOS of the fourth-layer C.

mixed slightly with Si 3p ($\sim$ 15%) (figure 9(*B*) 'c'; figure 9(*C*) 'e'). The overall surface C 2s-like orbital shifts to higher-energy states than that in the bulk (dashed line in figure 9(*B*) and (*D*)).

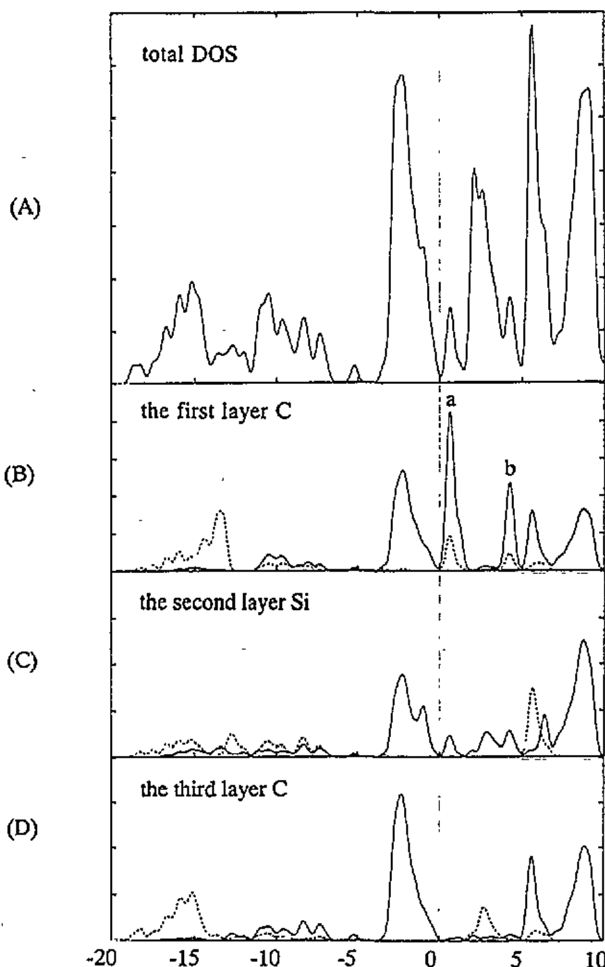

Figure 11. The DOS of the β-SiC(111) ideal C terminated surface; solid lines are p-like orbitals and dashed lines are s-like orbitals. (*A*) The total DOS; (*B*) the LDOS of the first-layer C; (*C*) the LDOS of the second-layer Si; (*D*) the LDOS of the third-layer C.

4.2. The β-SiC(001) ideal Si terminated surface

For the Si terminated β-SiC(001) ideal surface, the slab unit cell is identical to that of the C terminated surface with Si substituting C and vice versa. Figure 10 illustrates the total DOS and the LDOS for this surface.

Compared to the C terminated surface, the first-layer Si exhibits the dangling bond state (figure 10(*B*) 'a') located at a higher energy level of 4.35 eV in the conduction band. It is again an almost pure Si 3p atomic orbital state. Since the Fermi level is at about 1.5 eV, this state is empty. If we compare this surface to the β-SiC(111) Si terminated surface, on which each surface atom has only one dangling bond, we can see, once again, that the surface dangling state of the (111) surface is closer to the molecular Si sp^3 hybrid orbital state than that of the ideal β-SiC(001) surface. Similarly, the broadening of the dangling peak is due to the coupling of the dangling bonds of the same atom and of different surface atoms.

The hybridized surface state (figure 10(*B*) ‘b’; figure 10(*C*) ‘d’) is composed of Si 3p (~ 55%), Si 3s (~ 20%), and C 2p (~ 25%) orbitals. This state is due to the interaction between the surface Si and the second-layer C, similar to that of the C terminated surface. Since the Fermi level is at about 1.5 eV, this surface state is partially filled, and the surface can be characterized as a metallic surface. We note that the metallic characters of both C and Si terminated surfaces emerging from our calculations are in agreement with Lu *et al*’s predictions [23].

On the other hand, unlike the C terminated surface, there is no surface state in the ionicity gap for the Si terminated surface. Instead, the surface states, contributed mainly by the Si 3s orbital, appear from −9 eV to −6 eV in the upper valence band (figure 10(*B*) ‘c’).

In both C and Si terminated surface cases, the third and the inner layers exhibit essentially the bulk band structure, indicating that the surface does not have much effect on the inner layer electronic structure. However, electron transfer does affect the charge distribution up to a few layers below the surface. For the C terminated surface, because the first-layer C has higher band structure energy than the bulk C, many electrons fill back to the bulk C atoms, hence the surface Si and C are not as ionic as those in the bulk. For the Si terminated surface, however, a large number of electrons go into the second-layer C atoms from the surface Si atoms, because the surface Si is in higher-energy states. In this case, surface Si and C are much more ionic than those in the bulk. Table 5 shows the first- and the second-layer atomic charges. It should be pointed out that our calculation does not include self-consistency, thus our results for atomic charges can only be regarded as qualitative.

The *experimental work of angular resolved valency band photoemission spectroscopy* for β-SiC(001) performed by Hoechst *et al* [31] clearly indicates that in the fundamental gap, at about 1.0 eV below E_F, the photoemission feature is due to the existence of surface states. Note that their β-SiC sample is n type and the Fermi level is measured at about 2.0 ± 0.1 eV above the uppermost valency band, therefore the occupied state in their case should be at about 1.0 eV above the valency band maximum. Since the surface is not well characterized in their experiments, both Si and C could be present on the surface: the Fermi level in the experiment could be in between the Fermi levels of the perfect C terminated and Si terminated surfaces. This is consistent with our results that the Fermi levels of ideal C terminated and ideal Si terminated surfaces are 0.5 eV and 1.5 eV above the valency band maximum, respectively. Moreover, they have attributed the non-dispersive peak in their spectrum at about −9.8 eV binding energy to the indirect transition from flat band regions around X, W, and K points of the third band. This agrees well with our calculation, which shows that the bottom of the third band is at about −10 eV (figure 1(*A*)). Direct transition from the s-like valency band below the third valency could not be observed in their spectra because of the limited energy range they used (14–24 eV).

4.3. The β-SiC(111) ideal C terminated surface

As mentioned earlier, the bonding environment of the atoms on this surface is close to sp^3 hybridization, except that each surface atom loses one of its four nearest neighbours (figure 3), leaving a non-bonding hybrid on the surface. In the molecular limit, the C sp^3 hybridization energy is approximately $(E_s + 3E_p)4$ [36, 48], i.e. −0.52 eV. Compared to the (001) surface this C surface dangling level (figure 11(*B*) ‘a’) is closer to the molecular C sp^3 hybrid state. Of course, the surface dangling state is not the ideal molecular C sp^3 hybrid, because the surface non-bonding hybrid is influenced by the back bonds and by other non-bonding hybrids on the surface. Therefore, its energy level is shifted to a slightly

Table 5. The first- and the second-layer atomic charges (in electrons).

	(001) ideal (1 × 1)		(111) ideal (1 × 1)[a]		(110) ideal (1 × 1)	(001) (2 × 1)	(001) (3 × 2)	(100) (2 × 2) staggered	(100)(2 × 2) bridged
First-layer charges	C: −0.22	Si: 0.53	C: −0.22	Si: 1.12	C: −1.17 Si: 1.09	Si: 0.57	Si: 0.42[b]	C: −0.41	C: −0.99
Second-layer charges	Si: 0.47	C: −0.85	Si: 0.50	C: −1.34	C: −0.53 Si: 0.58	C: −0.87	C: −0.81	Si: 0.72	Si: 1.16

[a] The same slab unit cell containing an Si terminated surface and a C terminated surface on the top and the bottom of the slab, respectively, is used; there exists electron transfer from the Si surface to the C surface, therefore the interpretation of these calculated values should be cautious.

[b] Averaging the first and the second surface Si layers.

higher energy level than the ideal C molecular sp^3 hybrid level, centred at 0.6 eV and is composed of C 2p (~ 70%), C 2s (~ 15%), and Si 3p (~ 15%). The corresponding antibonding state of this hybridized state is peak 'b' in figure 11(*B*).

4.4. The β-SiC(111) ideal Si terminated surface

The atomic configuration of this surface is similar to the (111) ideal C terminated surface (figure 3), except that Si substitutes for C, and vice versa.

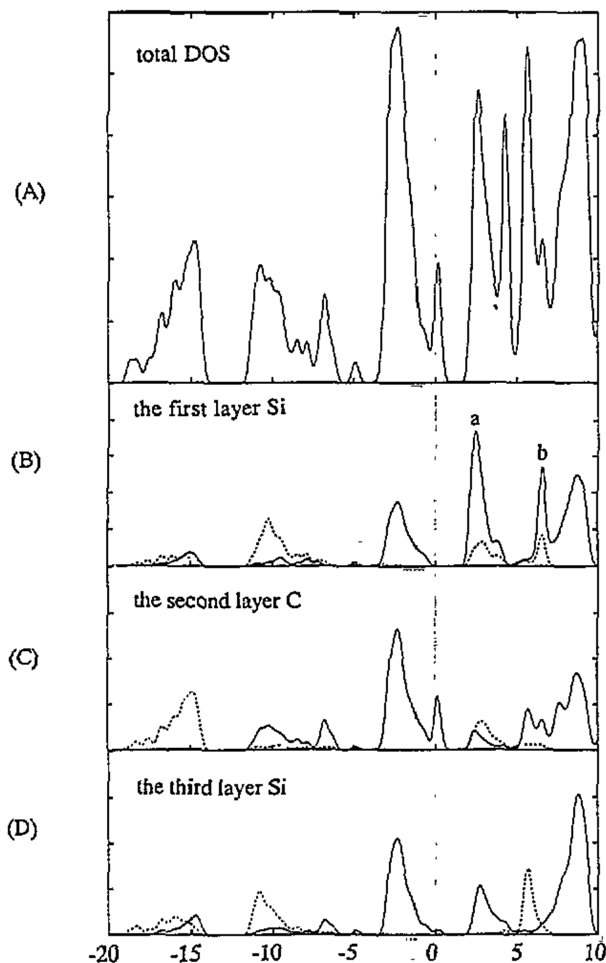

Figure 12. The DOS of the β-SiC(111) ideal Si terminated surface; solid lines are p-like orbitals and dashed lines are s-like orbitals. (*A*) The total DOS; (*B*) the LDOS of the first-layer Si; (*C*) the LDOS of the second-layer C; (*D*) the LDOS of the third-layer Si.

Similar to the ideal (111) C terminated surface, this surface dangling state is not a pure Si 3p orbital, but an Si sp^3 hybridized state (figure 12(*B*) 'a'). The Si molecular sp^3 hybridization level is at about 2.05 eV. However, the sp^3 hybridization of the surface atom is not complete due to the absence of the fourth neighbour. This unbonded sp^3 hybrid orbital will interact with the back bonds and other unbonded hybrids on the surface, leading to a shift toward higher energy levels and the delocalized surface dangling bond states, centred at about 2.5 eV, right at the conduction band minimum. Compared to the β-SiC(001) Si terminated surface, this dangling bond energy level shifts to a lower level by about 1.85 eV. This state is composed of Si 3p (~ 70%), Si 3s (~ 15%), and C 2p (~ 15%). Its antibonding state corresponds to peak 'b' in figure 12(*B*).

4.5. The β-SiC ideal (110) surface

β-SiC(110) is a non-polar surface (figure 4), consisting of both Si and C atoms. In figure 13, we present the calculated total DOS and LDOSs.

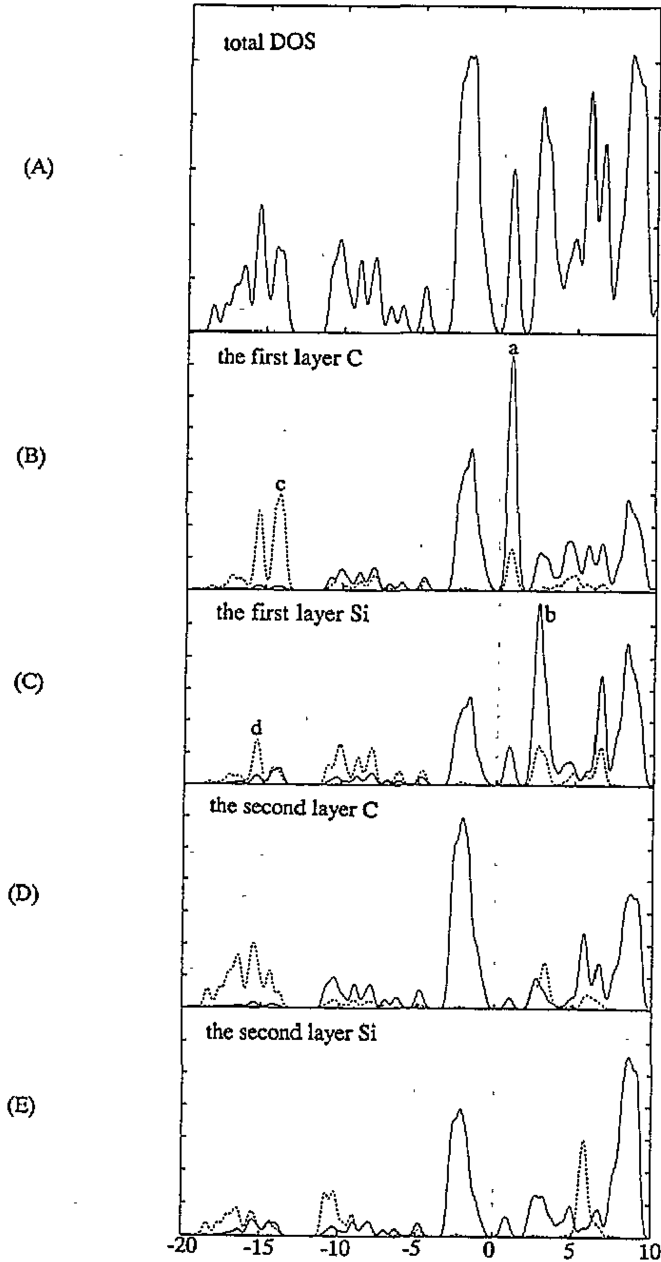

Figure 13. The DOS of the β-SiC(110) ideal surface; solid lines are p-like orbitals and dashed lines are s-like orbitals. (*A*) The total DOS; (*B*) the LDOS of the first-layer C; (*C*) the LDOS of the first-layer Si; (*D*) the LDOS of the second-layer C; (*E*) the LDOS of the second-layer Si.

A significant feature of the ideal β-SiC(110) surface DOS is the existence of two hybrid surface states, located just above the top of the valency band (figure 13(*B*) 'a') and at the edge of the conduction band minimum (figure 13(*C*) 'b'), which can be attributed to the C sp^3 hybridized dangling bond (C 2p ($\sim$ 75%), C 2s ($\sim$ 12.5%), and Si 3p ($\sim$ 12.5%)) and the Si sp^3 hybridized dangling bond (Si 3p ($\sim$ 75%), Si 3s ($\sim$ 15%), and C 2p ($\sim$ 10%)), respectively. This agrees well with the findings of Lee and Joannopoulos [22]. Because there is only one dangling bond per C or Si atom, the energy level of which is very close to that on the corresponding (111) surface, a localized surface state at about -14 eV contributed mainly by the C 2s orbital, extends slightly from the upmost edge of the first band into the ionicity gap (figure 13(*B*) 'c' and figure 13(*C*) 'd'). This is also consistent with the calculation of Lee and Joannopoulos, in which the surface band at about -15% eV, although mostly in the ionicity gap, is found to diffuse into the upper edge of the first band.

On the (110) surface, both Si and C atoms are in higher-energy states than they are in the bulk. The surface C atoms, however, have much lower-energy states with respect to the surface Si atoms, thus a significant number of electrons transfer to the surface C atoms from the surface Si atoms. This makes the β-SiC(110) ideal surface very ionic (table 5).

4.6. The β-SiC(001) (2 $\times$ 1) surface

This surface is believed to be terminated with 1 ML Si. The atomic configuration of the surface is illustrated in figure 5. The total DOS and LDOS calculated from this model are shown in figure 14.

There is only one dangling bond left on each surface Si atom, similar to the (111) Si terminated surface. The dangling bond 'a' in figure 14 is basically sp^3 hybridized. Its energy level, centred at about 2.3 eV, is close to the Si molecular sp^3 orbital, which is at 2.05 eV. The antibonding state of this dangling bond hybridization is associated with peak 'b'. Both the hybridized dangling state and its antibonding state are shifted slightly to lower energies compared to those of the (111) surface, due to the occurrence of Si–Si dimerization on the (2 $\times$ 1) surface. Influenced by the back bonds, this dangling bond is further mixed with the back bonds (figure 14(*C*) 'k', 'l'). The interaction between these dangling bonds on different atoms causes the dangling state peak to broaden.

Again, compared to the (111) ideal Si surface, the appearance of Si–Si dimerization gives rise to Si–Si bonding (σ), represented by the states 'c' and 'e' in figure 14; the corresponding antibonding states (σ^*) are 'd' and 'f'. The states 'e' and 'f' basically originate from the Si 3s interaction, while 'c' and 'd' mainly arise from the Si 3p interaction, although s–p hybridization is evident. There are also interactions between the Si–Si dimer bond and the back bonds, reflected in figure 14 by the peaks 'g', 'h', 'i', and 'j'.

Mehandru and Anderson [21] have studied the relaxation of the Si terminated β-SiC(001) (2 $\times$ 1) surface, using the TB atom superposition and electron delocalization band technique. They have also found the same mechanism for the change of electronic structure due to the (2 $\times$ 1) reconstruction. They illustrate that when an Si–Si σ bond is formed, the corresponding antibonding orbital is pushed up high in energy, and each surface Si is now left with one dangling surface state orbital, which rehybridizes and results in a new surface state band. Robertson [38] has found that the Si–Si bond gives a resonance feature in the Si s-like band at -10.2 eV, which corresponds to our Si 3s bonding orbital at -11.3 eV.

The Fermi energy level is at about 2.25 eV, and the dangling bond state is partially filled. As mentioned above, the model we use for the (2 $\times$ 1) reconstruction is a symmetric Si dimer model, because of the nature of the empirical potential, but if we adopt the model of Craig and Smith [24] and Powers *et al* [20], it is expected that the dangling bond state 'a' will split into two dangling bond states due to the buckled dimers, in analogy to the well

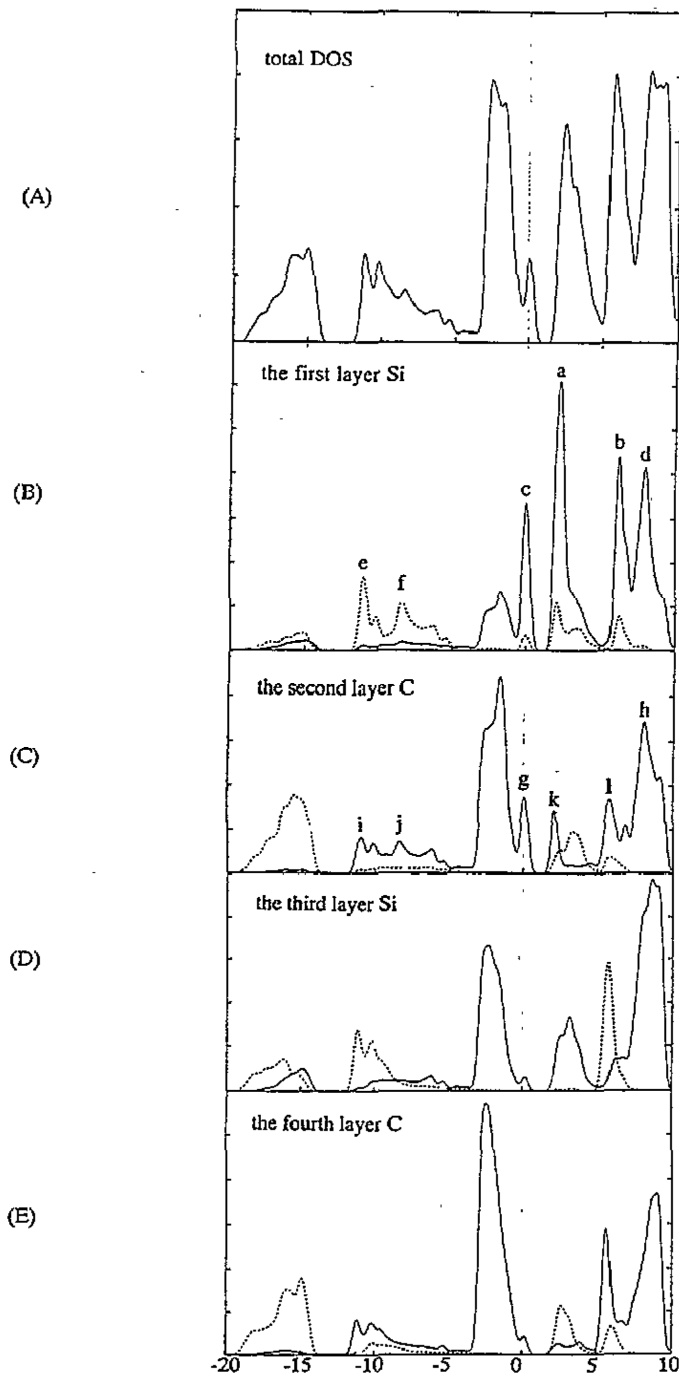

Figure 14. The DOS of the Si terminated (001) (2 × 1) surface; solid lines are p-like orbitals and dashed lines are s-like orbitals. (*A*) The total DOS; (*B*) the LDOS of the first-layer Si; (*C*) the LDOS of the second-layer C; (*D*) the LDOS of the third-layer Si; (*E*) the LDOS of the fourth-layer C.

known Si(001) (2×1) surface buckled Si dimer model. On the Si(001) (2×1) surface, the band with lower energies corresponds to the up atom of the dimer, while the band with higher energy levels to the down atom. The electrons will then fill the lower dangling band and leave the upper dangling band empty, rendering the surface semiconducting. Comparing the β-SiC (2×1) surface to the Si (2×1) surface and keeping in mind that the dangling bond of this β-SiC surface could split if a dimer tilting occurs in reality, we can see that the electronic structure of this Si terminated β-SiC(001) (2×1) surface becomes similar to that of the Si(001) (2×1) surface. Kruger *et al* [53] have performed a first-principles electronic structure calculation for the Si(001) (2×1) surface and found that the two dangling bond orbitals, lying just below and above the Fermi energy level (π bonding and antibonding characters) are contributed by the Si $3p_z$ orbital, which is also rehybridized with the Si 3s orbital. Moreover, another surface resonance state lying further below the Fermi level is contributed by the Si $3p_x$ and $3p_y$ orbitals (σ bonding). These features of the Si(001) (2×1) surface correlate well with our calculation for the Si terminated SiC(001) (2×1) surface.

The experimental work of ARUPS (angular resolved ultraviolet photoelectron spectroscopy) and APUBIS (angular resolved ultraviolet bremsstrahlung isochromat spectroscopy) by Himpsel and Fauster [54] reveals the same electronic structure for the Si(001) (2×1) surface. Uhrberg *et al* [55] have also concluded from their experimental studies on the Si(001) (2×1) surface that, besides the dangling bond surface states at 0.7 eV below E_F, there is a dimer bridge bond surface state ranging between 2 and 3 eV below E_F. This is consistent with our calculated Si dimer bond state of the β-SiC(001) (2×1) surface, which is about 2.25 eV below E_F.

4.7. The β-SiC(001) (3×2) reconstructed surface

As described earlier, this surface has an excess $\frac{1}{3}$ ML Si atoms on top of the Si terminated surface. The atomic model proposed by Hara *et al* and adopted in our calculation is illustrated in figure 6. The total DOS is similar to that of the β-SiC(001) (2×1) surface. Figure 5 shows only the LDOS of the surface.

This surface should have characteristics similar to those of both the β-SiC(001) (2×1) surface and the Si(001) (2×1) surface. There are, however, four atomic groups on the surface, which have different bonding environments. These groups are designated in figure 6. For the atoms of groups I, II, and IV, there is one dangling bond per atom and the corresponding Si sp^3 hybridized dangling bonds are the states 'a', 'g', and 's', respectively (figure 15(A), (B), and (D)), resembling those on the β-SiC ideal (111) and (001) (2×1) surfaces. The corresponding antibonding states of these dangling states are 'b', 'h', and 't', respectively. For group III, the Si atom forms four bonds to its non-ideally tetrahedral neighbours, yet the Si sp^3 hybridization is not complete, and the remaining 3s and 3p orbitals interact with the hybridized dangling bonds of its neighbours, giving rise to the weakly hybridized dangling-like state 'm' in figure 15(C), with 'n' being the corresponding antibonding state. Although we utilize a symmetric dimer model, asymmetric dimers on the (3×2) surface are also possible, in analogy to the Si(001) (2×1) surface as well as in terms of the interpretation of the LEED pattern [14]. Hence, these dangling state bands may split into two bands, one below and one above the Fermi level.

The major difference between this surface and the β-SiC(001) (2×1) surface is that because of two missing dimer rows and the dimerization of the sublayer Si atoms, the Si–Si bond lengths and orientations in different groups of atoms are quite different, inducing the shifting and broadening of the Si–Si pσ bonding states, originally centred at 0.0 eV on the (2×1) surface. For group I, the nearest neighbours of each atom are all Si atoms. This causes the surface Si–Si pσ bonding state to shift to a higher energy level centred at about

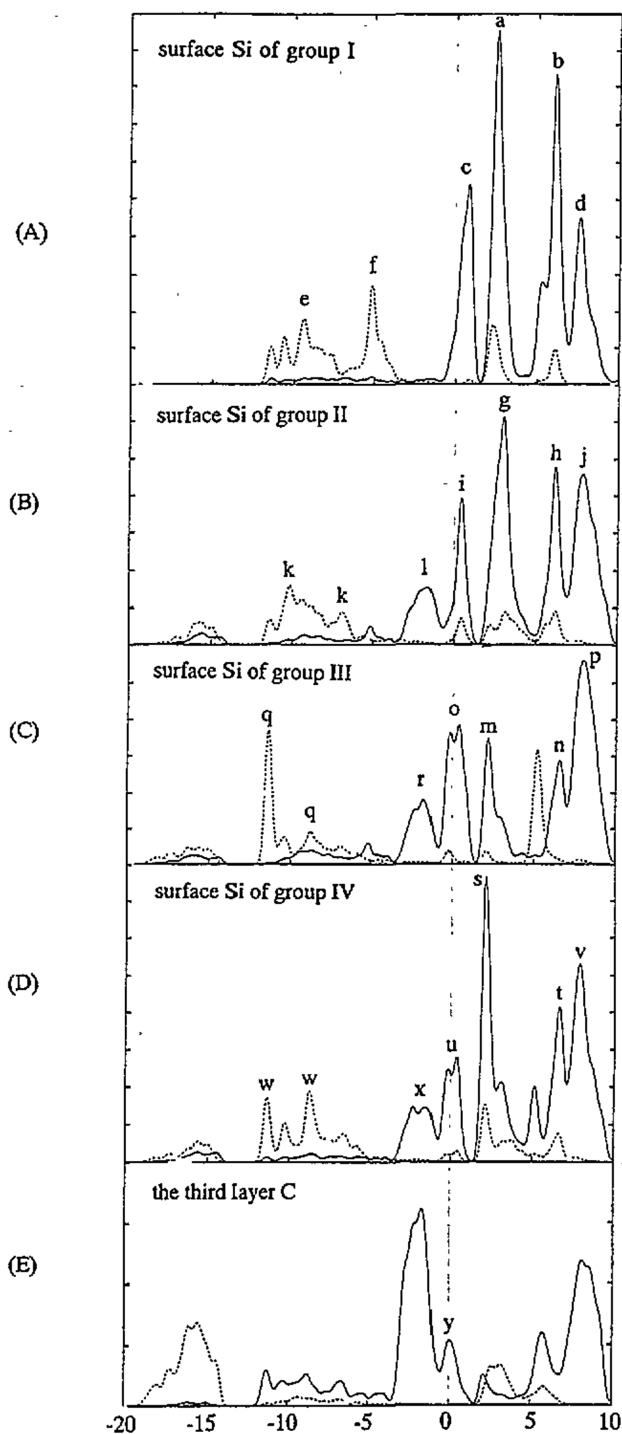

Figure 15. The DOS of the Si terminated (001) (3×2) surface; solid lines are p-like orbitals and dashed lines are s-like orbitals. (*A*) The LDOS of surface Si of group I; (*B*) the LDOS of surface Si of group II; (*C*) the LDOS of surface Si of group III; (*D*) the LDOS of surface Si of group IV; (*E*) the LDOS of the third-layer C.

1.8 eV (figure 15(*A*) 'c'). The group II atoms, having Si–C back bonds, also have an uplift of their Si–Si pσ bonding energy, although not as high as those of the topmost Si atoms (figure 15(*B*) 'i'). The group III and IV atoms, possessing Si–Si dimer bonds parallel to the surface plane and Si–C back bonds, similar to those on the β-SiC(001) (2 × 1) surface, centre their Si–Si pσ bonding states at about 0.0 eV again (figure 15(*C*) 'o'; figure 15(*D*) 'u'). We conclude that if an Si–Si bond is surrounded by more neighbouring Si–Si bonds and/or by fewer neighbouring Si–C bonds, the energy levels of the pσ states become higher, and vice versa. A similar trend occurs for the Si sσ states. For group I and II atoms, the Si sσ bonding states are located in a relatively higher-energy region (figure 15(*A*) 'e', 'f'; figure 15(*B*) 'k'), while the sσ bonding states of group III and IV atoms are closer to those of the (2 × 1) surface atoms (figure 15(*C*) 'q'; figure 15(*D*) 'w').

The 'd', 'j', 'p', and 'v' states are the corresponding antibonding states of the pσ bonding states. Notably, for the group I atoms, the pσ^* antibonding states (figure 15(*A*) 'd') shift slightly to lower energy levels. Recalling that the Si–Si pσ bonding states shift to higher levels, we can see that the Si–Si pσ bonding and pσ^* antibonding states become closer than those on the β-SiC(001) (2 × 1) surface, indicating a weaker topmost Si–Si dimer bonding than that on the (2 × 1) surface.

In addition, the bulklike Si–C bonding bands 'l', 'r', and 'x' can be attributed to the direct Si–C interactions in groups II, III, and IV, respectively. The Fermi level of this surface is at about 2.34 eV. Similar to the β-SiC(001) (2 × 1) surface, the Si–Si pσ bonding states are about 1.5–2.34 eV below E_F, comparable with that observed on the Si(001) (2 × 1) surface.

The overall feature of the (3 × 2) surface observed in experiments agrees with our calculation. Parrill and Chung [10] have found a clear indication of Si–Si bonding and that both Mg excited and Zr excited Si 2p spectra are shifted and broadened for the (3 × 2) surface. They attribute the broadening to surface oxidation. We add that, according to our calculation, the surface Si–Si bonds with different environments induced by the missing Si dimer rows may also account for the shifting and broadening of the Si–Si bonding state.

4.8. The β-SiC(001) c(2 × 2) surface—the staggered model

Since there is no conclusive evidence from experiment to discriminate between the staggered model and the bridged model, both models of the c(2 × 2) reconstruction are examined and compared. In figure 7, we show the unit cell and the top view for the staggered model. The total DOS and LDOS calculated based on this model are shown in figure 16.

On this surface, the C atoms are considered to be sp^3 hybridized, leaving one sp^3 hybridized dangling bond on the surface. The bonding and antibonding states of this hybridization correspond to the states 'a' and 'd', respectively, in figure 16(*B*). Compared to the C terminated (001) ideal surface, where the dangling state is pure C 2p orbital, the dangling state on this surface is hybridized with the C 2s orbital and gives rise to a band due to the coupling of the dangling bonds.

The C–C dimer bonding is represented by 'b' and 'e' in figure 16(*B*), which are of pσ and pσ^* bond characters, respectively. The peaks 'g' and 'h', on the other hand, correspond to the sσ and sσ^* dimer bonding states, respectively. We will see in the following that the C–C dimer bond of this surface is less strong than that of the bridged model surface.

The bond between the surface C and the sublayer Si deviates from ideal bulk bond length and angle, hence the resulting back bond states, corresponding to 'c' and 'k', and their antibonding states, corresponding to 'f' and 'l' in figure 16(*B*) and (*C*), are distinguishable with respect to the bulk states.

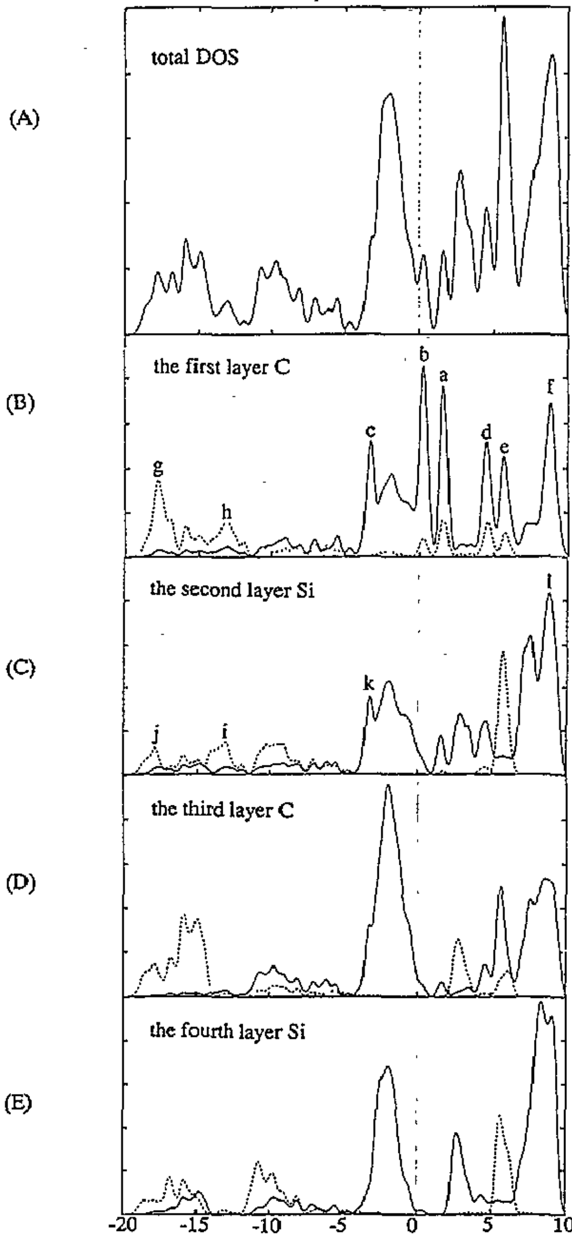

Figure 16. *The* DOS *of C terminated (001) (2 × 2) surface—the staggered model; solid lines* are p-like orbitals and dashed lines are s-like orbitals. (*A*) The total DOS; (*B*) the LDOS of the first-layer C; (*C*) the LDOS of the second-layer Si; (*D*) the LDOS of the third-layer C; (*E*) the LDOS of the fourth-layer Si.

Some experimental results seem to support this model. Bermudez and Kaplan [16] were able to prepare a homogeneous C terminated surface by adsorption of excess C on, rather than desorption of Si from, an initially stoichiometric surface and characterize these surfaces by using AES, ELS, and LEED. Their ELS spectra clearly show the evidence of a dangling

C bond, but no evidence of either a C=C double bond or a sublayer Si dangling bond. No characteristics of sp^2 hybridized or π bonded surface C are found in the experiments. Instead, the existence of sp^3 hybridization and direct dimer σ bonding is clearly indicated. The authors also point out that a weaker dangling bond pairing cannot be ruled out, although it is not a major effect to stabilize the c(2 × 2) structure. The overall experimental picture agrees with our calculation of this model quite well. The present model is also supported by Craig and Smith's calculation using a slab-MINDO molecular orbital method [56].

4.9. The β-SiC(001) c(2 × 2) surface—the bridged model

The atomic configuration of this surface is shown in figure 8. Two of the surface C atoms sit in the bridge site in between two sublayer Si atoms. Each sublayer Si atom bonds to three nearest-neighbour C atoms leaving one bond dangling. The total DOS and LDOS are shown in figure 17.

Since the surface C has only two nearest neighbours, the tetrahedral environment does not exist. Therefore, the surface C is more like that on the ideal (001) C terminated surface. The C dangling bond state should be a pure 2p orbital. However, the shorter dimer distance, 1.54 Å, compared to that of the staggered model (table 4) makes the dangling bond interaction stronger. Peaks 'a' (π) and 'c' (π^*) in figure 17 represent strong dangling bond pairing. This is the most significant difference between this surface and all other surfaces. Since the original dangling bonds are not hybridized, their pairing does not involve the C 2s orbital. Usually the π bond is induced by the interaction between pure p orbitals, and the energy difference between the π bonding and π^* antibonding is much less than that between σ and σ^* states. Therefore the fact that, in figure 17, 'a' and 'c' are completely contributed by the first-layer C p orbital, with no second-layer atomic orbitals participating in these two states, and that the splitting energy is much less than that of a σ bond (figure 17 'b' and 'e') suggests that these two peaks are of π and π^* characters.

The σ bonds of the C dimer should be associated with 'b' (pσ) and 'e' (pσ^*), as well as 'g' (sσ) and 'h' (sσ^*), in figure 17(B). This feature is in good analogy to that of the C=C bond calculated by Robertson [38], who used the same method as ours to study amorphous Si–C alloy. Moreover, the σ bonding and σ^* antibonding states 'b' and 'e' (figure 17(B)) in this model are much further apart than those of the staggered model (figure 16(B) 'b','e'), indicating the C dimer bond (C=C double bond) on this surface is much stronger than the C dimer bond (C–C single bond) on the staggered model surface.

Again, because the bond length and bond angle of the C–Si back bonds deviate from those of the ideal bulk bonds, the resulting back bond states 'd' and 'l' (both at σ type) and 'f' and 'j' (both are σ^* type) are prominent in figure 17(B) and (C).

Another significant feature of this surface is the appearance of a hybridized Si sp^3 dangling bond 'i', which is located at a slightly higher energy level than an ideal molecular sp^3 level due to the influence of the neighbouring bonds.

The overall electronic feature of this model, especially the presence of the Si dangling bond and C=C bond, is not supported by the experiments of Bermudez and Kaplan [16] or of Parrill and Chung [10]. Nevertheless, Powers *et al*'s [20] dynamic LEED I–V analysis of the β-SiC(001) c(2 × 2) surface and Badziag's [19] self-consistent total energy MNDO calculation favour the present bridged model.

5. Summary

We have calculated the electronic structures of β-SiC(001) reconstructed surfaces for all the proposed models, using an empirical TB method.

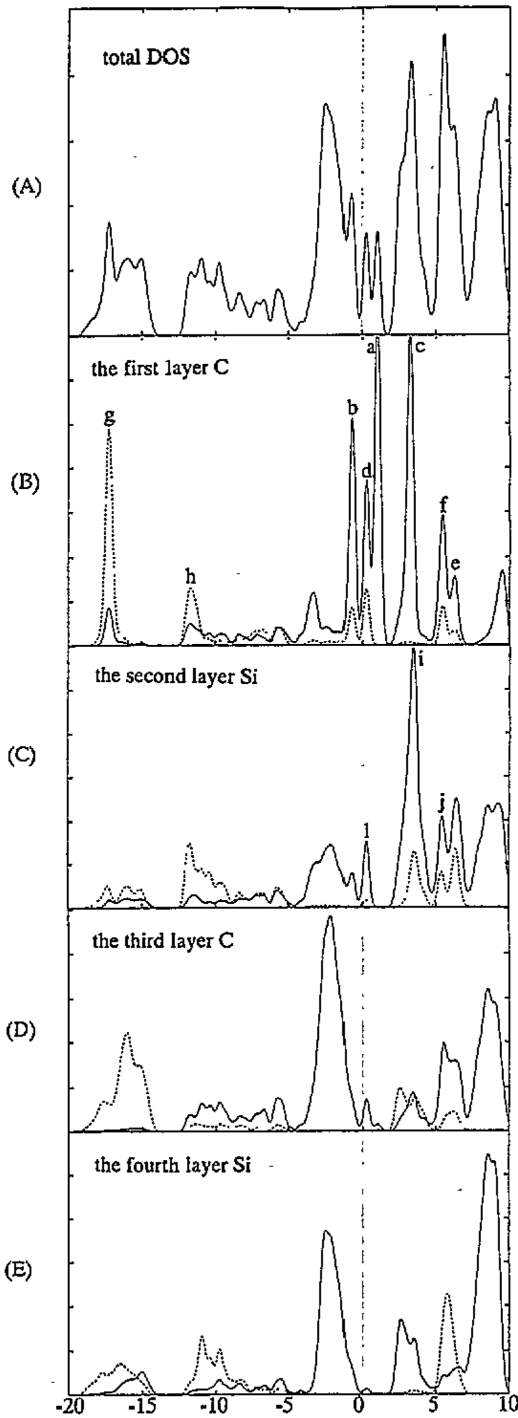

Figure 17. The DOS of the C terminated (001) (2×2) surface—the bridged model; solid lines are p-like orbitals and dashed lines are s-like orbitals. (*A*) The total DOS; (*B*) the LDOS of the first-layer C; (*C*) the LDOS of the second-layer Si; (*D*) the LDOS of the third-layer C; (*E*) the LDOS of the fourth-layer Si.

The (2×1) reconstruction of the β-SiC(001) surface is associated with an Si terminated stoichiometric surface. The surface Si exhibits an sp^3 hybridized dangling bond, similar to that of the Si(111) ideal surface. Surface Si dimerization gives rise to an Si–Si σ bond.

This surface resembles the Si(001) (2×1) surface. Our calculated Si dimer $p\sigma$ bonding state correlates with the experimental Si dimer bridge bond state of the Si(001) (2×1) surface reasonably well. However, because of the nature of the Keating empirical potential employed in obtaining our surface geometry of relaxation, we were unable to investigate the surface electronic structure with tilted Si dimers, which would have caused a splitting of the dangling bond band, as in the case of the Si(001) (2×1) surface.

The β-SiC(001) (3×2) reconstructed surface is comparable to the β-SiC(001) (2×1) surface in terms of their electronic structures. However, because of the missing Si dimer rows in the topmost excess Si layer and the sublayer Si atom dimerization, the surface Si–Si bond lengths and the bond angles are quite varied for different groups of surface atoms, causing the Si–Si σ bond surface states to shift and broaden in response to the respective bonding environment. For the same reason, the hybridized Si sp^3 dangling bond states, including those of the sublayer Si atoms, are also shifted and broadened. The topmost Si dimer bond of this surface is less strong than that on the (2×1) surface.

For the β-SiC(001) $c(2 \times 2)$ surface, it is found that, in the staggered model, the surface has a hybridized C sp^3 dangling bond state. The σ bond is found to be responsible for surface C dimerization. The C–C single dimer bond on this surface, however, is less strong than that on the bridged model surface. There is no Si dangling bond on this surface. On the other hand, the bridged model predicts a strong C 2p dangling bond pairing, giving rise to the π bonding and π^* antibonding states. The σ bond of the C pair is considered to be a C=C double bond. A hybridized Si sp^3 dangling bond also appears. While some experiments and calculations [16, 56] strongly support the staggered model, other studies [20, 19] favour the bridged model.

Acknowledgments

This work was partially supported by the University of Washington Graduate Research Fund.

References

[1] Dayan M 1985 *J. Vac. Sci. Technol.* A 3 361; 1986 *J. Vac. Sci. Technol.* A 4 38
[2] Muehlhoff L, Choyke W J, Bozack M J and Yates J T Jr 1986 *J. Appl. Phys.* 60 2842
[3] Munch W U and Pettenpaul E 1977 *J. Appl. Phys.* 48 4823
[4] Choyke W J 1987 *Proc. Novel Refractory Semiconductors (MRS Symp. Proc. 97)* ed D Emin, T L Aselage and C Wood (Pitsburgh, PA: Materials Research Society) p 207
[5] Powell A 1987 *Proc. Novel Refractory Semiconductors (MRS Symp. Proc. 97)* ed D Emin, T L Aselage and C Wood (Pittsburgh, PA: Materials Research Society) p 159
[6] Parker D A 1989 *Designing Interfaces for Technological Applications: Ceramic–Ceramic, Ceramic–Metal Joining* ed S D Peteves (New York: Elsevier) p 3
[7] Kraft W (ed) 1987 *Joining Ceramics, Glass and Metals* (Baa Nanheim, Germany: Informationsgesellschaft Verlag) pp 81, 89, 179, 191, 297, 369
[8] Ruhle M, Evans A G, Ashby M F and Hirth J P (ed) 1990 *Metal–Ceramic Interface Acta–Scr. Metall. Proc. Series 4* (New York: Pergamon) p 129, 138, 176
[9] Lee D J, Vaudin M D, Handwerker C A and Kattner U R 1988 *Mater. Res. Soc. Symp. Proc.* vol 120 (Pittsburgh, PA: Materials Research Society) p 357
[10] Parrill T M and Chung Y W 1991 *Surf. Sci.* 243 96
[11] Hara S, Slijkerman W F J, van der Veen J F, Ohdomari I, Misawa S, Sakuma E and Yoshida S 1990 *Surf. Sci.* 231 L196
[12] Hara S, Aoyagi Y, Kawai M, Misawa S, Sakuma E and Yoshida S 1992 *Surf. Sci.* 273 437

[13] Kaplan R and Parrill T M 1986 *Surf. Sci.* **165** L45
[14] Kaplan R 1989 *Surf. Sci.* **215** 111
[15] Kaplan R 1988 *J. Vac. Sci. Technol.* A **6** 829
[16] Bermudez V M and Kaplan R 1991 *Phys. Rev.* B **44** 11 149
[17] Yoshinobu T, Izumikawa I, Mitsui H, Fuyuki T and Matsunami H 1991 *Appl. Phys. Lett.* **59** 2844
[18] Cheng C S, Zheng N J, Tsong I S T, Wang Y C and Davis R F 1991 *J. Vac. Sci. Technol.* B **9** 681
Cheng C S, Tsong I S T and Davis R F 1991 *Surf. Sci.* **256** 354
[19] Badziag P 1991 *Phys. Rev.* B **44** 11 143
[20] Powers J M, Wander A, Rous P J, Van Hove M A and Somorjai G A 1991 *Phys. Rev.* B **44** 11 159; 1992 *Surf. Sci. Lett.* **260** L7
[21] Mehandru S P and Anderson A B 1990 *Phys. Rev.* B 42 9040
[22] Lee D H and Joannopoulos J D 1982 *J. Vac. Sci. Technol.* **21** 351
[23] Lu W C, Yang W and Zhang K 1991 *J. Phys.: Condens. Matter* 3 9079
[24] Craig B I and Smith P V 1990 *Surf. Sci.* **233** 255
[25] Takai T, Halicioglu T and Tiller W A 1985 *Surf. Sci.* **164** 341
[26] Chadi D J 1979 *Phys. Rev. Lett.* **43** 43; 1979 *J. Vac. Sci. Technol.* **16** 1290
[27] Ihm J, Cohen M L and Chadi D J 1980 *Phys. Rev.* B **21** 4592
[28] Tin M T and Cohen M C 1981 *Phys. Rev.* B **24** 2303
[29] Zhu Z, Shima N and Tsukada M 1989 *Phys. Rev.* B **40** 11 868
[30] Parrill T M and Bermudez V M 1987 *Solid State Commun.* **63** 231
[31] Hoechst H, Tery M, Johnson B C, Meere J M, Zajac G W and Fleish T H 1987 *J. Vac. Sci. Technol.* A **5** 1640
[32] Chadi D J 1978 *Phys. Rev. Lett.* **41** 1062
[33] Vogl P, Hjalmarson H P and Dow J D 1983 *J. Phys. Chem. Solids* **44** 365
[34] Hemstreet L A Jr and Fong C Y 1971 *Solid State Commun.* **9** 643; 1972 *Phys. Rev.* B **6** 1464
[35] Talwar D N and Feng Z C 1991 *Phys. Rev.* B 44 3191
[36] Harrison W A 1980 *Electronic Structure and The Properties of Solids* (San Francisco, CA: Freeman)
[37] Majewski J A and Vogl P 1987 *Phys. Rev.* B **35** 9666
[38] Robertson J 1992 *Phil. Mag.* B **66** 615
[39] Slater J C and Koster G F 1954 *Phys. Rev.* B 94 1498
[40] Harrison W A and Froyen S 1980 *Phys. Rev.* B **21** 3214
[41] Chadi D J 1977 *Phys. Rev.* B **16** 3572
[42] Chadi D J 1989 *Atomistic Simulation of Materials Beyond Pair Potentials* ed V Vitek and D J Scrolovitz (New York: Plenum)
[43] Artacho E and Yudurain F 1989 *Phys. Rev. Lett.* **62** 2491
[44] Batra I P 1990 *Phys. Rev.* B **41** 5048
[45] Pandey K C 1984 *Proc. 17th Int. Conf. on the Physics of Semiconductors* ed D J Chadi and W A Harrison (New York: Springer) p 55
[46] Martins J C and Zunger A 1984 *Phys. Rev.* B **30** 6217
[47] Kohyama M 1993 Private communication
[48] Lanno M and Friedel P (ed) 1991 *Atomic and Electronic Structure of Surfaces* (New York: Springer)
[49] Keating P N 1966 *Phys. Rev.* B **145** 637
[50] Martin R M 1970 *Phys. Rev.* B **1** 4005
[51] Kohyama M, Kose S, Kinoshita M and Yamamoto R 1990 *J. Phys.: Condens. Matter* **2** 7809; Kohyama M, Kose S and Yamamoto R 1991 *J. Phys.: Condens. Matter* **3** 7555
[52] Lubinsky A R, Ellis D E and Painter G S 1975 *Phys. Rev.* B **11** 1537
[53] Kruger P, Mazur A, Pollmann J and Wolfgarten G 1986 *Phys. Rev. Lett.* **57** 1468
[54] Himpsel F J and Fauster Th 1984 *J. Vac. Sci. Technol.* A **2** 815
[55] Uhrberg R I G, Hansson G V, Nicholls J M and Flodstrom S A 1991 *Phys. Rev.* B 24 4684
[56] Craig B I and Smith P V 1991 *Surf. Sci. Lett.* **256** L609